DOI: 10.1039/D3MH00013C (Communication) *Mater. Horiz.*, 2023, **10**, 1274-1281

Deep-learning based spatio-temporal generative model on assessing state-of-health for Li-ion batteries with partially-cycled profiles †

Seojoung Park ‡, Hyunjun Lee ‡, Zoe K. Scott-Nevros, Dongjun Lim, Dong-Hwa Seo, Yunseok Choi *, Hankwon Lim * and Donghyuk Kim *

School of Energy and Chemical Engineering, Ulsan National Institute of Science and Technology (UNIST), 50 UNIST-gil, Eonyang-eup, Ulju-gun, Ulsan, 44919, Republic of Korea. E-mail: dkim@unist.ac.kr

Received 4th January 2023 , Accepted 14th February 2023

First published on 20th February 2023

Abstract

Accurately estimating the state-of-health (SOH) of lithium-ion batteries is emerging as a hot topic because of the rapid increase in electric appliance usage. However, versatile applicability to various battery compositions and diverse cycling conditions, and prediction only with partial data still remain challenges. In this paper, a Deep-learning-based Graphical approach to Estimation of Lithium-ion batteries SOH (D-GELS) was developed to predict the SOH covering three cathode materials, $LiFePO_4$, $LiNiCoAlO_2$, and $LiNiCOMnO_2$. D-GELS shows an accurate performance for SOH prediction, less than 0.012 of RMSE, was predicted regardless of cathode materials, and its applicability was confirmed. Furthermore, D-GELS was capable of predicting the SOH using partially-cycled data, since less than 0.046 of RMSE was observed even with 50% of the image missing. When using partially-cycled profiles, significant economic benefits can be

seen in used battery management, as the number of assessed batteries increases greatly, leading to cost savings.

New concepts

This research focuses on the estimation of the state of health for Li-ion batteries *via* a deep learning framework. The newly-developed model was trained with spatio-temporal data based on voltage, current, and temperature cycling profiles, which removes the reliance of the model on an expert's insight for feature engineering. Additionally, it can estimate the state of health regardless of the cathode material used, of those included in the training dataset, and covers various cycling conditions. Notability, a spatio-temporal approach can be applied to the deep generative model to reconstruct the partially cycled dataset. The previous studies have limitations on feature engineering, as an expert's insight is needed for feature extraction and selection, require fully-cycled datasets, and can only analyze limited cycling conditions. Further, the prior studies have focused on a specific type of cathode material, which cannot cover the compositional behavior of battery charging and discharging, in spite of continuous reports about the component and ratio of a metallic element. The presented framework is not bound by either of these constraints.

1. Introduction

Li-ion batteries have been widely used as energy storage for power sources in portable devices, such as cell phones and electric vehicles, due to their high energy density and effortless management.[1–3] Additionally, their application is expected to expand as the importance of renewable energy increases.[4] In response to this issue, an interest in battery management systems (BMS), battery health prognostics and management, is also increasing.[5,6] However, there are several technical barriers to accurately predicting the state-of-health (SOH) and remaining useful life (RUL) due to complex aging mechanisms.

Previous research modeled Li-ion batteries to predict the SOH and RUL using a semi-empirical model. The semi-empirical model was used to describe physical and electrochemical phenomena, such as loss of lithium inventory and loss of active material in electrodes, indicating capacity degradation in Li-ion batteries for SOH assessment.[7–9] Moreover, a combination of a particle filter and

the semi-empirical model showed successful SOH prediction.[9–11] Based on the development of computing ability and ease of data access, data-driven methods, such as machine learning and deep learning, were proposed for SOH estimation. This study focused on the correlation between measured data and SOH, unlike the semi-empirical model. For machine learning models, XGBoost,[12] support vector regression (SVR),[12,13] Gaussian process regression (GPR),[13–16] and Elastic net[17] were suggested. For deep learning models, recurrent neural network (RNN),[13] convolutional neural network (CNN),[13] encoder–decoder,[18] long short-term memory network (LSTM),[19] and deep neural network (DNN),[20] were proposed to predict SOH. However, each data-driven model presented in prior research is restricted to a single cathode material, $LiFePO_4$ (LFP),[14,17] $LiNiCoAlO_2$ (NCA),[12–14,18] $LiNiCOMnO_2$ (NMC),[12,14,16,19] $LiCoO_2$ (LCO),[13,18,20] and lead–acid battery.[15]

Previous research has demonstrated successful performance in battery SOH estimation *via* data-driven approach. However, to the best of the authors' knowledge, SOH estimation models covering multiple chemical compositions of electrodes have been scarcely investigated, since cycling data, such as voltage (V), current (I), and temperature (T) vary depending on cathode composition and operating conditions. Therefore, the estimation models, feature engineering-based SOH regression in previous studies, have limitations in dealing with cycling profiles under various conditions. In this paper, we focus on a battery SOH estimation framework without any expert insight or feature processing by spatio-temporal approaches that spatialized voltage, current, and temperature cycling profiles. The dataset from the Sandia National Laboratories (SNL) which includes the fully-cycled profiles of NMC, LFP, and NCA batteries was used. To estimate the battery SOH, the spatio-temporal channels, which were converted from cycling profiles, were fed into the CNN regression model, which is called "Deep-learning based Graphical approach to Estimation of Lithium-ion batteries SOH" (D-GELS) (Fig. 1a). The performance of D-GELS was verified by comparing the results from the D-GELS framework to results from conventional models, such as GPR, SVR, Random Forest (RF), and Stochastic Gradient Descent (SGD).

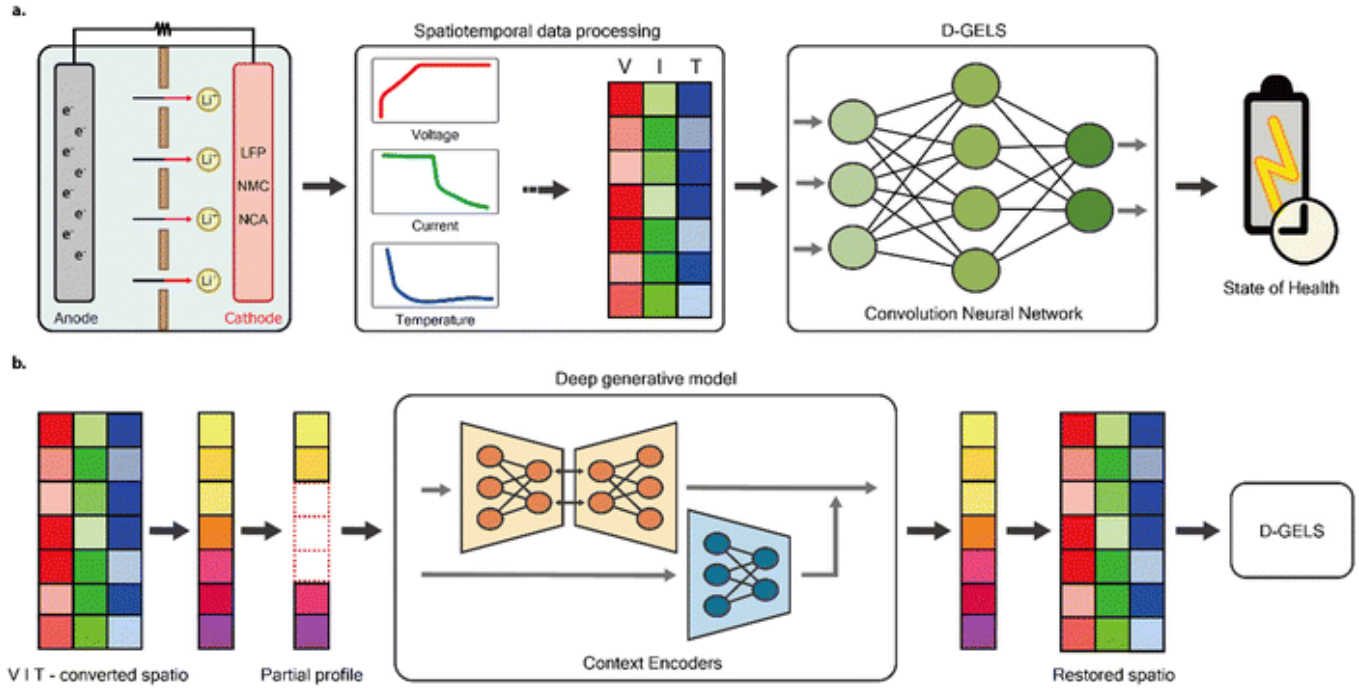

Fig. 1 Overview of the proposed structure, D-GELS. (a) The schematic diagram of SOH estimation *via* D-GELS includes the conversion process of spatio-temporal channels from voltage, current, and temperature profiles. (b) The schematic diagram of SOH estimation with restoring missing images from a partially-cycled profile using D-GELS.

Moreover, the greater part of recent feature engineering-based models is based on fully cycled profiles, despite that most electric appliances in everyday use are only charged and discharged partially. Hence, the central challenge of recent studies is the estimation of SOH using partially cycled profiles. Under this challenge, Richardson *et al.* demonstrated the maximum capacity estimation model using time values at equispaced voltage points[21] and Tian *et al.* designed a convolution neural network that estimates the maximum and remaining capacities with only short-term charging data.[22] However, these approaches take cycling profiles over time step as input, which is difficult to cover multiple cycling data that vary depending on operating conditions. The spatiotemporal approach of D-GELS allows us to overcome this shortcoming by viewing temporal data in spatial dimension when designing an estimation model on partial cycling profiles.

Hence, in this paper, a new approach is suggested to develop a SOH estimation model using partial charge and discharge profiles depending on the percentage of information missing. The partial-cycling dataset, which contains missing information, was restored by feeding it into the deep generative model, Context Encoders, and the limitation of requiring a fully-cycled profile was overcome. As shown in Fig. 1b, the restored data was fed into D-GELS to predict the SOH. Finally, economic benefits were explored when SOH could be estimated using a partially-cycled dataset compared to a fully-cycled dataset.

2. Methods

The voltage, current, cell temperature cycling profiles were converted into (n, 1, 3)-dimensional spatio-temporal channels, where n is the number of measurement points in one cycle. They were resized to (128, 1, 3)-dimensional images and normalized for each cycle for feeding into D-GELS. It was performed in python using OpenCV and sklearn packages. This study used CNN, which can make use of strengths of spatio-temporal approaches, to construct a deep learning framework to estimate the SOH of lithium-ion batteries. CNN architecture is widely applied in computer and machine vision space, such as handwriting recognition[23] and waste classification,[24] due to its outstanding performance in image processing. It considers deep information from the input image by extracting the features from small subregions and captures the relationship between input and output labels.[25] In this paper, the input and output are spatio-temporal channels and SOH, respectively. A typical CNN model consists of three types of layers: convolution layers, pooling layers, and fully connected layers. The convolution layers act as a filter that produces feature maps of the input channels and reduces noise. Eqn (1) shows how the convolution layer is performed. In this equation, the lth convolution layer is y^l_{ij}. The activation function is represented by σ, the bias for the jth feature map is equal to b^l_j, the weight of the kernel is $w^l_{m,j}$, the index value of the filter is represented by m, and the output of the $(l-1)$th convolution layer is $x^{l-1}_{i+m-1,j}$.

$$y^l_{ij} = \sigma\left(b^l_j + \sum_{m=1}^{M} w^l_{m,j} x^{l-1}_{i+m-1,j}\right) \tag{1}$$

The pooling layer reduces the dimensions of the maps that have been passed through convolution, thus reducing the amount of information in features. As shown in eqn (2), maximum pooling is selected as the pooling function. In this equation, the output of the lth pooling layer is represented by p^l_{ij}, the output of the (l-1)th convolution layer is equal to $y^{l-1}_{i\times s+r,j}$, the pooling size is R, and the stride is represented by s.

$$p^l_{ij} = y^{l-1}_{i\times s+r,j} \tag{2}$$

Finally, the fully connected layer is used to classify channels into predetermined labels based on the results of previous layers.

In our CNN regression model, the layer of convolution is adopted to map the relations between V, I, T-converted channels, and the lithium-ion battery SOH. And the model consists of two stages (ESI† Fig. S7a). First, the convolution operation is performed through a linear activation function, ReLU. Then the

maximum pooling process is performed on the results. Two layers of convolutional networks and fully connected layers were used, and the dropout rate was set to 25% and 50%, respectively for regulation.

The second step of D-GELS is image restoration. The Context Encoders are utilized to restore the original *V*, *I*, *T*-converted channels from the partially inpainted ones. It has an architecture composed of a generator and a discriminator. The generator consists of both a decoder and an encoder that can fill in missing portions of an image using channel information. The generator and discriminator are trained competitively with each other.

In our deep generative model, the encoder has five convolutional layers and ReLU for activation functions to extract (4, 1, 512)-dimensional latent feature space from (128, 1, 3) input. On the other hand, the decoder consists of multiple transposed convolutional layers so that it can perfectly restore the missing parts from the latent space dimension. The transposed operations are performed through ReLU as activation functions except for in the last layer, which uses the Hyperbolic Tangent function. The generator constructed in this way creates a fake spatial channel by mimicking the original one. The discriminator consists of multiple convolutional layers that decide whether the generated channel is true or not. The deep learning models for D-GELS were constructed in Python using Keras, Tensorflow, and Sklearn packages.

D-GELS was trained on 70% of the data randomly extracted from the dataset and validated using 70% of the unused data from the dataset. The remaining data was used to test the model performance. To evaluate the performance of the CNN regression model, three error metrics, RMSE, MAE, and MAPE were calculated as follows:

$$\mathrm{RMSE} = \sqrt{\frac{\sum_{i=1}^{n}(y_i - \hat{y}_i)^2}{n}} \tag{3}$$

$$\mathrm{MSE} = \frac{\sum_{i=1}^{n}(y_i - \hat{y}_i)^2}{n} \tag{4}$$

$$\mathrm{MAE} = \frac{\sum_{i=1}^{n}|y_i - \hat{y}_i|}{n} \tag{5}$$

where, y_i is the predicted value, $\hat{y}_i$ is the measured value, and n is the total number of samples.

3. Results

Since battery cycle profiles have distinct patterning depending on cathode composition, we tried to break away from the conventional feature engineering-based approach. In this novel workflow we are presenting, the voltage, current, and cell temperature cycling profiles were converted into (128, 1, 3)-dimensional spatio-temporal channels (Fig. 2a). To implement this approach, a total of 17 090 cycling profiles consisting of four commercial 18 650 cells each for LFP, NCA, and NMC at experimental conditions (25 °C, 0.5C-rate for discharge, and 1C-rate for charge), were used.[26,27]

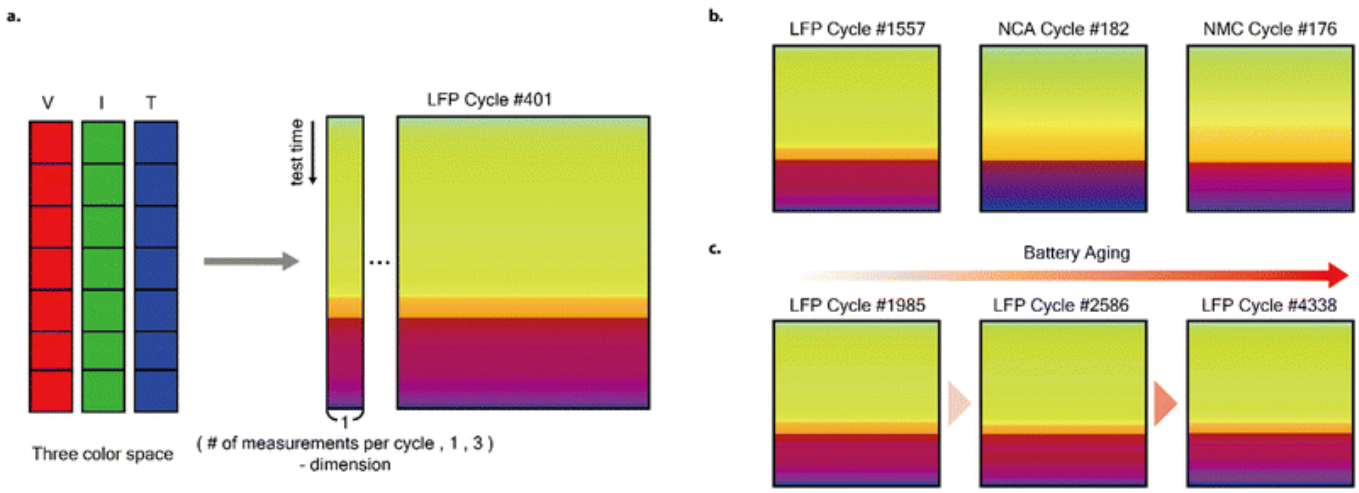

Fig. 2 The *V*, *I*, *T*-converted spatio-temporal channels with *x*-axis extended to (128, 128, 3) for visualization. (a) The process of generating the *V*, *I*, *T*-converted channels. The time-series profiles, *V*, *I*, and *T* were mapped to red, green, and blue channels, respectively, and converted into (the number of measurements per cycle, 1, 3)-dimensional images. The spatio-temporal channels were then resized to (128, 1, 3)-dimensional images. (b) The variation of channels due to cathode material LFP, NCA, and NMC. (c) The gradual transition of channels as the battery undergoes aging in the LFP case.

Examples of converted channels are presented in Fig. 2b. As expected, the color distribution patterns were visually distinct depending on the cathode material, consistent with varying chemical properties. Additionally, there were minute changes in the distribution patterns as the battery aged, with the LFP case shown in the Fig. 2c. In the current data-driven approach, the variation in patterning between different cathode materials impedes SOH estimation. Therefore, we employed a deep learning-based approach to evaluating SOH of a battery regardless of cathode composition.

To predict the SOH of Li-ion batteries, a Convolution Neural Network (CNN) was proposed in D-GELS. The convolution layers were expected to capture the relationship between the spatio-temporal channels and the SOH as labels. Battery aging was successfully estimated at about 0.01 of RMSE. The performance of our CNN model was presented with the box-and-whisker plot in Fig. 3a. It shows outstanding performance in terms of three error metrics, 0.0088 of RMSE, 0.0066 of MAE, and 0.0072 of

MAPE. Furthermore, the individual cathode material channels in test data uniformly indicate estimation performance, less than 0.0115 of RMSE without significant deviation. As shown in Fig. 3b, estimated SOH was almost identical to reference SOH, and there were no extreme outliers.

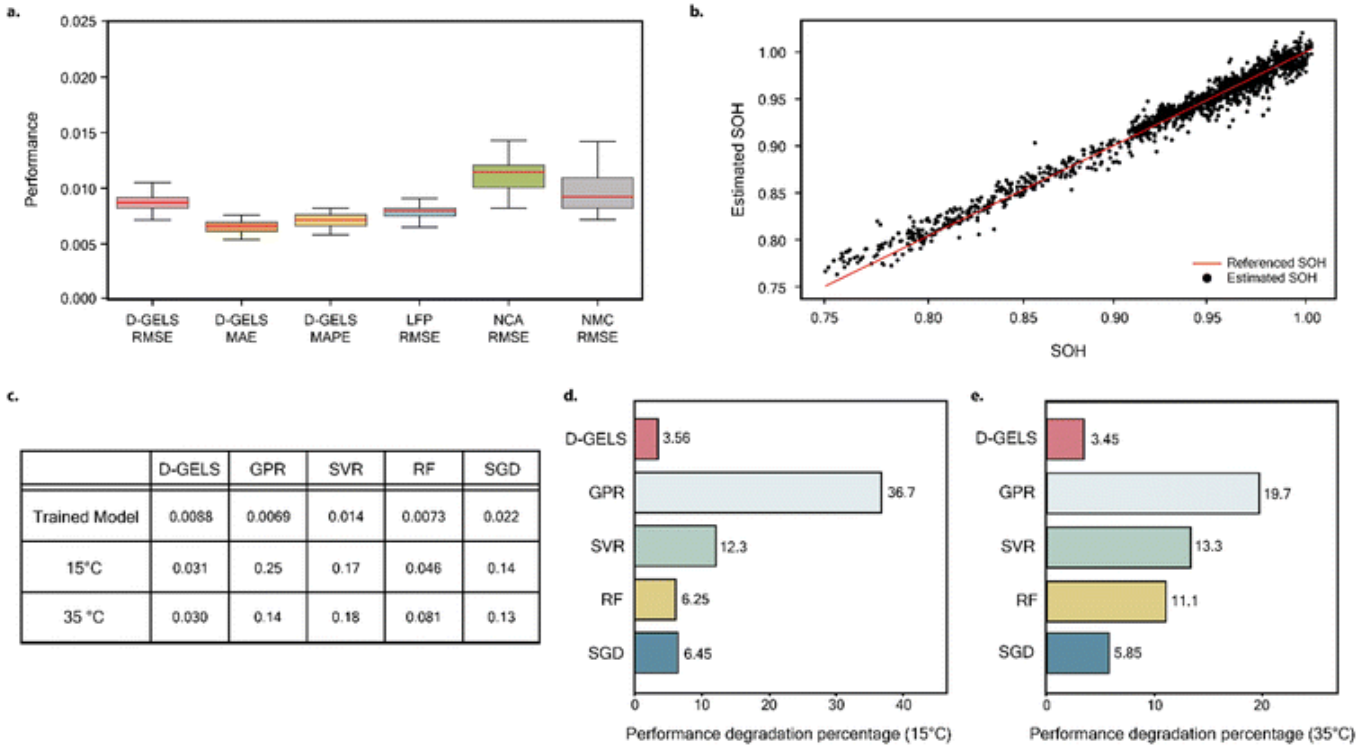

	D-GELS	GPR	SVR	RF	SGD
Trained Model	0.0088	0.0069	0.014	0.0073	0.022
15°C	0.031	0.25	0.17	0.046	0.14
35 °C	0.030	0.14	0.18	0.081	0.13

Fig. 3 Outstanding performance of D-GELS in SOH estimation. (a) High SOH estimation performance of D-GELS in terms of three error metrics: RMSE, MAE, and MAPE. RMSEs depicted separately depending on cathode materials (LFP, NCA, NMC). (b) Observed and estimated SOH from D-GELS. (c) Comparative analysis of D-GELS and feature-based conventional approach in terms of RMSE. The models were trained with 25 °C cycling profiles and applied to 15 °C, and 35 °C test data. (d) Comparison of percent difference in RMSE between the trained model and model applied to 15 °C cycling data between D-GELS and conventional frameworks. (e) Comparison of percent difference in RMSE between the trained model and model applied to 35 °C cycling data between D-GELS and conventional frameworks.

To verify remarkable D-GELS performance and general applicability, a comparative analysis of D-GELS and conventional frameworks was conducted. The conventional models were constructed with feature-based approaches. Firstly, features were extracted from cycling profiles and optimal subsets were selected for estimating SOH. Then, subsets were fed into regression models, GPR, SVR, RF, and SGD (ESI† Note S1). D-GELS and the conventional frameworks were trained with 25 °C cycling data and applied to different test cycling conditions, 15 °C and 35 °C. Both performances, in terms of RMSE and

the difference between values under test cycling conditions and training conditions, were compared (Fig. 3c–e). Training performances were presented for all cases in terms of RMSE, all less than 0.03, and the lowest RMSE was observed with GPR. However, limitations have been revealed in applying conventional models to test data under different cycling conditions. While the difference in RMSE values percentage for D-GELS was about 3.5% in both temperatures, the lowest value from the conventional models was 5.85%, SGD tested at 35 °C. The reason that D-GELS can be applied to other condition profiles is that *V*, *I*, *T*-converted channels reflect the profile tendency, unlike the conventional models trained with a subset of numerical feature values. These results showed the utility of D-GELS for accurate SOH estimation regardless of cathode composition and cycling condition.

To take advantage of our deep learning-based model, which can reflect the tendency of cycling profiles, we designed a deep-generative model that can estimate SOH with only partially-cycled profiles. Since it is time and labor intensive using the full cycling profiles to diagnose battery health, this approach will bring time and economic efficiency. The context Encoders, an advanced Generative Adversarial Network (GAN), was used to restore the partially-cycled profiles to fully-cycled profiles. As depicted in Fig. 4, the *V*, *I*, *T*-converted spatio-temporal channels with 12.5%, 25%, and 50% of the image missing were successfully restored. SOH estimation using a partial dataset was achieved by integrating the deep-generative model and CNN model in D-GELS.

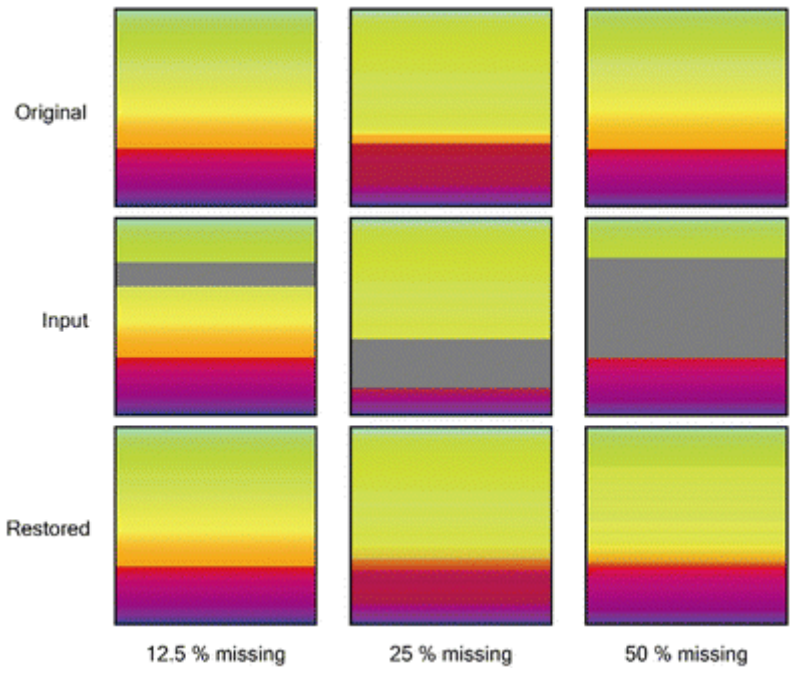

Fig. 4 Examples of restored spatio-temporal channels by a deep generative model. The original, input, and restored spatio channels when restoring input data with missing parts accounting for 12.5%, 25%, or 50% of the image at randomized positions.

As shown in Fig. 5a, D-GELS was capable of predicting SOH by restoring the random partial-cycling profiles. Although estimation performance degradation was shown with increasing percentage of the image missing, the successful estimation was indicated with RMSE values of 0.046 or less regardless of the percentage (ESI† Table S2). Furthermore, D-GELS showed outstanding SOH estimation regardless of whether it was early cycle data or data near End-of-Life (EOL) (Fig. 5b). Above all, most of the observed errors were negative, meaning the predicted SOH was below reference SOH, which is a significant part of diagnosing battery life. The exception to this trend was an observed estimation performance decrease after about 90% of SOH when 50% of the image was missing. This is when the Li-ions are plated.[28] Outliers are shown above the reference SOH because of a great amount of data loss that would indicate Li-ion plating. In addition, the effect of temporal characteristics of cycling profiles on the restored and estimation performance was also investigated by moving the missing windows by five pixels toward the end. As shown in Fig. 5c, performance degradation increased greatly when the missing window included the early discharge process. This was further supported in the observed lower performance when recovering 75% missing part, which excludes most of the early discharge stages, even compared to random size between 25% and 50% missing or two randomly spaced 25% windows (ESI† Fig. S14).

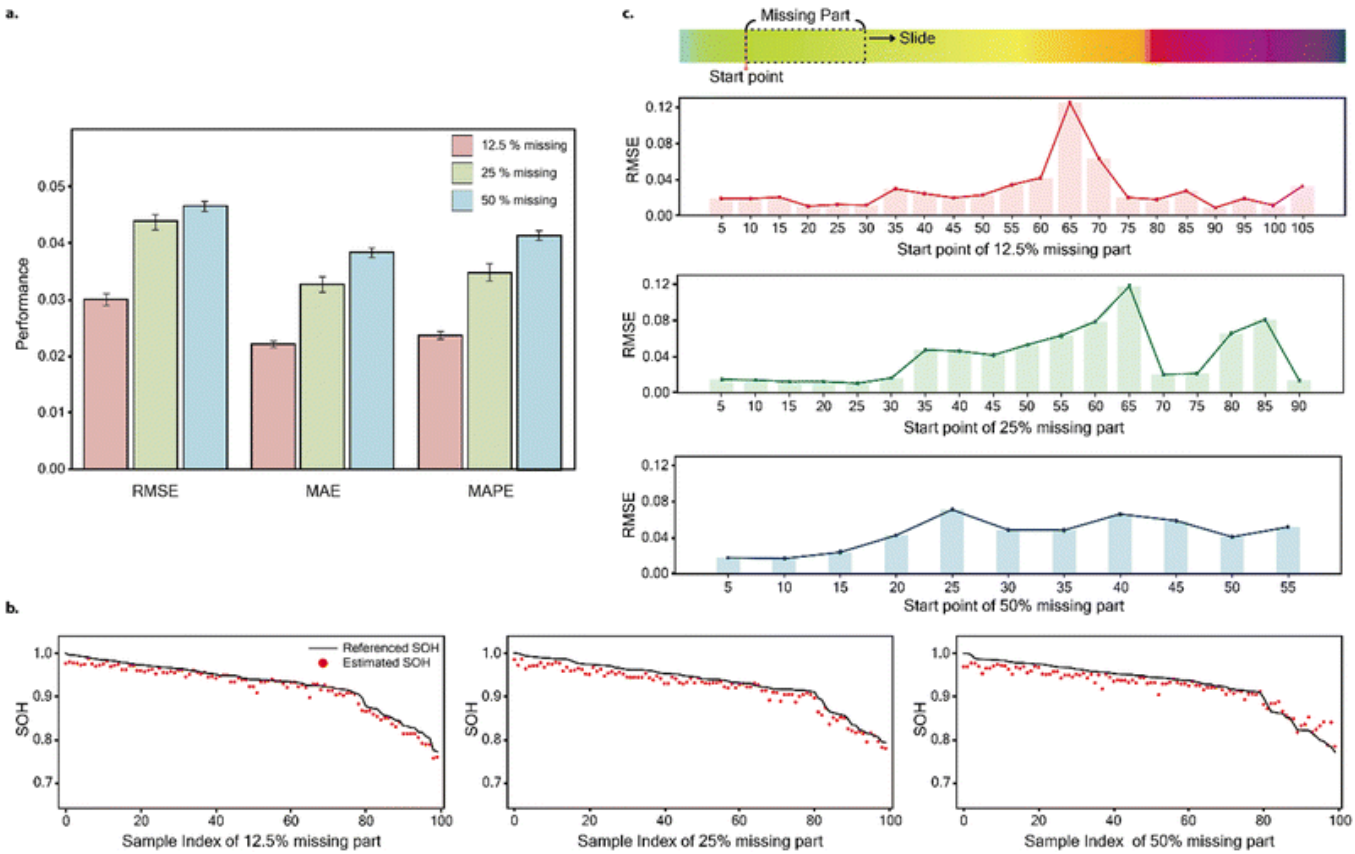

Fig. 5 The performance of D-GELS in SOH estimation with the restored partial-cycling profiles. (a) The performance of D-GELS in predicting SOH with partial-cycling data in terms of three error metrics:

RMSE, MAE, and MAPE. (b) Observed and estimated SOH degradation for each missing percentage, 12.5%, 25%, and 50%. (c) RMSE according to the initial position of the missing part, as the missing window is moved across the spatio-temporal channel from start to end. The red, green, and blue columns indicate the results from 12.5%, 25%, and 50% of the image missing, respectively.

The supply of used batteries is expected to increase as time passes due to the increased usage of electric appliances. Estimating the SOH is important for preparing for the 2nd life of the used battery. Hence, technical and economic benefits were investigated in terms of the amount of battery packs assessed in a year, and cost savings when predicting SOH using a partial dataset. 75% and 50% of data during cycling were considered and the cell configuration was assumed to be 96s1p and economic and technical parameters were presented in ESI† Table S10.[29]

As shown in Fig. 6a–c, it is useful to use a partially-cycled dataset to predict the SOH. Over 30% more batteries are predicted to be assessed in comparative analysis between 50% partially-cycled and fully-cycled, regardless of cathode materials. In addition, the cathode material that yielded the highest number of battery packs assessed was NMC, followed in order by NCA and LFP. In terms of economic benefit, the cost savings increased with a decrease in used data at about €100 per pack (Fig. 6d–f). Therefore, assessing battery packs using D-GELS with a partial dataset is an effective way to manage used batteries in the future.

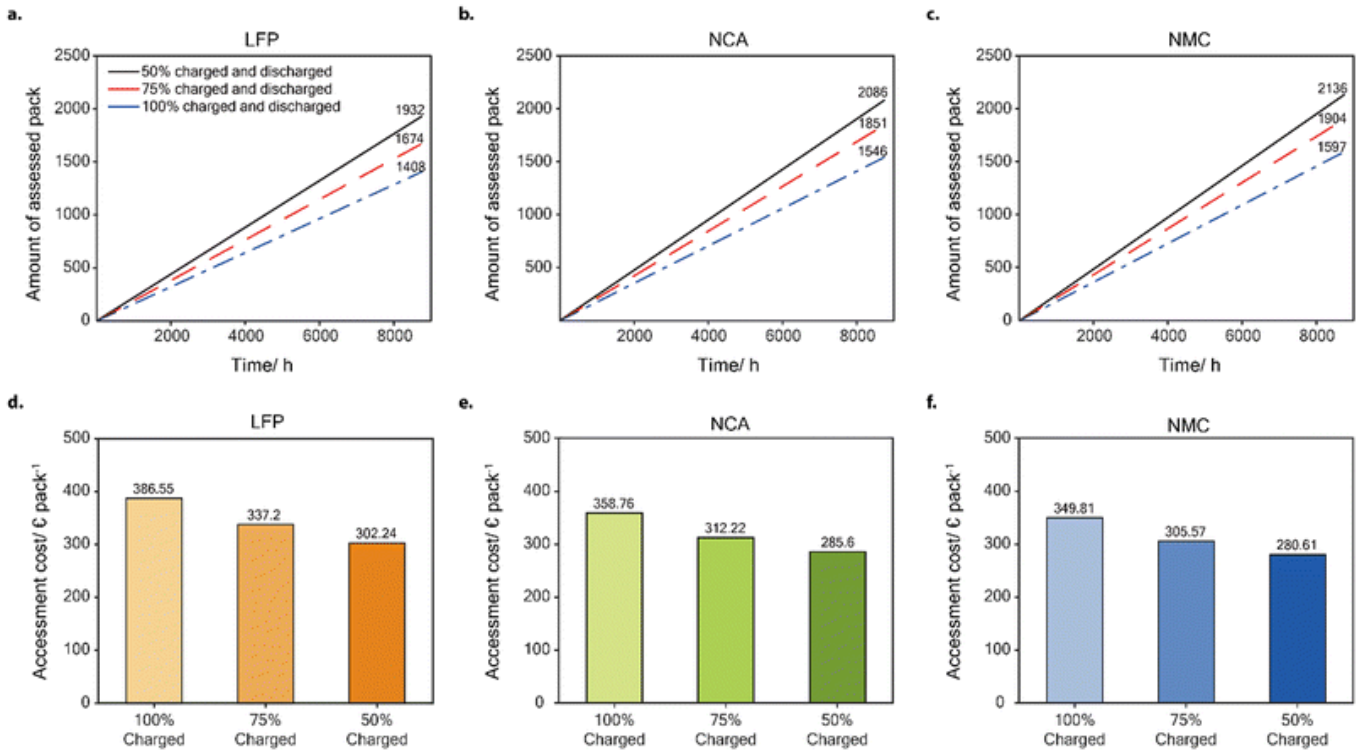

Fig. 6 The technical and economic benefits when SOH is predicted using a full dataset *versus* a partial dataset. (a–c) Total amount of battery packs assessed in a year depending on the ratio of used data and cathode compositions. (d–f) Cost savings of the assessment process depending on the ratio of used data and cathode compositions.

4. Conclusions

Deep learning-based SOH estimation models are emerging as a promising approach to diagnosing Li-ion battery lifetime due to its accurate and rapid estimation. Unfortunately, one challenge facing application of this estimation approach is that estimation is cathode-material-specific and requires certain cycling conditions, and that full cycling data must be used. This research proposed a general-purpose deep-learning framework with spatio-temporal data processing for a new approach to estimating the SOH of lithium-ion batteries called D-GELS (Deep-learning based Graphical approach to Estimation of Lithium-ion batteries SOH). The cycling profiles of voltage, current, and temperature from LFP, NCA, and NMC batteries were converted into spatio-temporal channels. The converted channels were fed into D-GELS to predict the SOH, and it showed accurate performance, less than 0.012 of RMSE. In addition, in comparative analysis with conventional frameworks, GPR, SVR, RF and SGD, D-GELS showed high applicability to various cycling temperature conditions.

Moreover, D-GELS showed outstanding performance in SOH estimation using partially cycled data. It restored randomly removed data, which accounted for 12.5%, 25%, or 50% of the image. It showed 0.030 of RMSE when 12.5% of the image was missing, and less than 0.046 of RMSE even when 50% of the image was missing. And it was clearly shown that the performance of D-GELS degraded over a certain range, which included the early discharge process. Thus, managing the discharge process is critical to estimating the SOH accurately. More than 30% of the amount of battery packs can be assessed, and costs can be reduced by about €100 when assessing a battery pack with only 50% of a fully-cycled profile. One of the big advantages of our approach in terms of environmental aspects is that it can contribute to reducing CO_2 emissions by a decrease in the amount of used electricity for the inspection of battery packs. Our proposed framework can be helpful in managing used batteries in the future by assessing the SOH using a partially-cycled dataset regardless of cathode composition and cycling conditions.

Author contributions

Conceptualization and methodology were prepared by S. Park and H. Lee. Software was constructed by S. Park. The manuscript was written by H. Lee and Z. K. Scott-Nevros. Data curation and visualization

were performed by D. Lim and D.-H. Seo. The manuscript was reviewed and edited by Y. Choi, D. Kim, and H. Lim, and H. Lim supervised the work.

Data availability

Data used in this study can be obtained from Battery Archive: https://batteryarchive.org.

Code availability

The code for data processing and D-GELS framework is available at https://github.com/SBML-Kimlab/D-GELS.git.

Conflicts of interest

There are no conflicts to declare.

Acknowledgements

This work was supported by Development of high-power capacitor (supercapacitor) performance enhancement technology customized for companies by the Ministry of Trade, Industry and Energy and Korea Evaluation Institute of Industrial Technology (Project No. 00155725), by the Technology Innovation Program funded by the Ministry of Trade, Industry & Energy (MOTIE) of the Republic of Korea (No. 20015820), and by the Agency for Defense Development by the Korean government (UD2200061D).

References

1. M. Mishra, J. Martinsson, M. Rantatalo and K. Goebel, *Reliab. Eng. Syst. Saf.*, 2018, **172**, 25–35 CrossRef Find It @ SNU .
2. V. Sulzer, P. Mohtat, A. Aitio, S. Lee, Y. T. Yeh, F. Steinbacher, M. U. Khan, J. W. Lee, J. B. Siegel, A. G. Stefanopoulou and D. A. Howey, *Joule*, 2021, **5**, 1934–1955 CrossRef Find It @ SNU .
3. L. Ren, L. Zhao, S. Hong, S. Zhao, H. Wang and L. Zhang, *IEEE Access*, 2018, **6**, 50587–50598 Search PubMed Find It @ SNU .
4. T. Li, F. Xing, T. Liu, J. Sun, D. Shi, H. Zhang and X. Li, *Energy Environ. Sci.*, 2020, **13**, 4353–4361 RSC Find It @ SNU .
5. J. Qu, F. Liu, Y. Ma and J. Fan, *IEEE Access*, 2019, **7**, 87178–87191 Search PubMed Find It @ SNU .
6. Y. Wang, J. Tian, Z. Sun, L. Wang, R. Xu, M. Li and Z. Chen, *Renewable Sustainable Energy Rev.*, 2020, **131**, 110015 CrossRef Find It @ SNU .

7. M. Varini, P. E. Campana and G. Lindbergh, *J. Energy Storage*, 2019, **25**, 100819 CrossRef Find it @ SNU .
8. K. Khodadadi Sadabadi, P. Ramesh, P. Tulpule and G. Rizzoni, *J. Energy Storage*, 2019, **24**, 100789 CrossRef Find it @ SNU .
9. J. Tian, R. Xu, Y. Wang and Z. Chen, *Energy*, 2021, **221**, 119682 CrossRef CAS Find it @ SNU .
10. B. Routh, A. Guha, A. Patra and S. Mukhopadhyay, 2021 IEEE International Conference on Prognostics and Health Management, ICPHM 2021 DOI: 10.1109/ICPHM51084.2021.9486635 .
11. Y. Lian, J. v Wang, X. Deng, J. Kang, G. Zhu and K. Xiang, Proceedings – IEEE International Symposium on Circuits and Systems DOI: 10.1109/ISCAS45731.2020.9180516/VIDEO .
12. J. Zhu, Y. Wang, Y. Huang, R. Bhushan Gopaluni, Y. Cao, M. Heere, M. J. Mühlbauer, L. Mereacre, H. Dai, X. Liu, A. Senyshyn, X. Wei, M. Knapp and H. Ehrenberg, *Nat. Commun.*, 2022, **13**(1), 1–10 CAS Find it @ SNU .
13. Y. Fan, F. Xiao, C. Li, G. Yang and X. Tang, *J. Energy Storage*, 2020, **32**, 101741 CrossRef Find it @ SNU .
14. Z. Deng, X. Hu, P. Li, X. Lin and X. Bian, *IEEE Trans. Power Electron.*, 2022, **37**, 5021–5031 Search PubMed Find it @ SNU .
15. A. Aitio and D. A. Howey, *Joule*, 2021, **5**, 3204–3220 CrossRef Find it @ SNU .
16. S. Khaleghi, Y. Firouz, J. van Mierlo and P. van den Bossche, *Appl. Energy*, 2019, **255**, 113813 CrossRef Find it @ SNU .
17. K. A. Severson, P. M. Attia, N. Jin, N. Perkins, B. Jiang, Z. Yang, M. H. Chen, M. Aykol, P. K. Herring, D. Fraggedakis, M. Z. Bazant, S. J. Harris, W. C. Chueh and R. D. Braatz, *Nat. Energy*, 2019, **4**(5), 383–391 CrossRef Find it @ SNU .
18. Q. Gong, P. Wang and Z. Cheng, *J. Energy Storage*, 2022, **46**, 103804 CrossRef Find it @ SNU .
19. Y. Liu, G. Zhao and X. Peng, *IEEE Access*, 2019, **7**, 155130–155142 Search PubMed Find it @ SNU .
20. L. Ren, L. Zhao, S. Hong, S. Zhao, H. Wang and L. Zhang, *IEEE Access*, 2018, **6**, 50587–50598 Search PubMed Find it @ SNU .
21. R. R. Richardson, C. R. Birkl, M. A. Osborne and D. A. Howey, *IEEE Trans. Industr. Inform.*, 2019, **15**, 127–138 Search PubMed Find it @ SNU .
22. J. Tian, R. Xiong, W. Shen, J. Lu and F. Sun, *Energy Storage Mater.*, 2022, **51**, 372–381 CrossRef Find it @ SNU .
23. E. Al-wajih and R. Ghazali, *Knowl. Based Syst.*, 2023, **259**, 110079 CrossRef Find it @ SNU .
24. T. W. Wu, H. Zhang, W. Peng, F. Lü and P. J. He, *Resour., Conserv. Recycl.*, 2023, **190**, 106813 CrossRef Find it @ SNU .

25. C. M. Bishop, *Pattern Recognition and Machine Learning*, Springer, 2006 Search PubMed Find It @ SNU .
26. G. dos Reis, C. Strange, M. Yadav and S. Li, *Energy AI*, 2021, **5**, 100081 CrossRef Find It @ SNU .
27. Y. Preger, H. M. Barkholtz, A. Fresquez, D. L. Campbell, B. W. Juba, J. Romàn-Kustas, S. R. Ferreira and B. Chalamala, *J. Electrochem. Soc.*, 2020, **167**, 120532 CrossRef CAS Find It @ SNU .
28. X. G. Yang, Y. Leng, G. Zhang, S. Ge and C. Y. Wang, *J. Power Sources*, 2017, **360**, 28–40 CrossRef CAS Find It @ SNU .
29. H. Rallo, G. Benveniste, I. Gestoso and B. Amante, *Resour., Conserv. Recycl.*, 2020, **159**, 104785 CrossRef Find It @ SNU .

Footnotes

† Electronic supplementary information (ESI) available. See DOI: https://doi.org/10.1039/d3mh00013c

‡ S. Park and H. Lee contributed equally to this work.